PHYSICAL REVIEW B VOLUME 27, NUMBER 8 15 APRIL 1983

Energy dependence of the carrier mobility-lifetime product in hydrogenated amorphous silicon

Warren B. Jackson and R. J. Nemanich
Xerox Palo Alto Research Center, 3333 Coyote Hill Road, Palo Alto, California 94304

Nabil M. Amer
Applied Physics and Laser Spectroscopy Group, Lawrence Berkeley Laboratory, University of California, Berkeley, California 94720

(Received 22 November 1982)

The results of optical-absorption measurements determined by photothermal deflection spectroscopy, primary photoconductivity, and secondary photoconductivity on undoped and phosphorus-doped hydrogenated amorphous silicon films (*a*-Si:H) are reported. A normalization procedure for obtaining photocurrent spectra at constant generation rate is demonstrated. From these measurements, the efficiency-mobility-lifetime product ($\eta\mu\tau$) for electrons is found to be constant from 2.0 to $\sim$0.9 eV for both undoped and phosphorus-doped *a*-Si:H. For excitations less than $\sim$0.9 eV, there is evidence that the product $\eta\mu\tau$ for electrons drops rapidly; similarly, the $\eta\mu\tau$ for holes exhibits a rapid decrease in undoped material for photon energies less than $\sim$1.5 eV. A model is proposed to explain the results, resolving a discrepancy between secondary- and primary-photoconductivity measurements of the optical absorption.

I. INTRODUCTION

Disorder significantly affects the transport properties of solids. One property that is significantly altered by disorder is the mobility μ. Extended states well within the conduction or valence band have a high mobility while localized states within the band gap possess an extremely low mobility. The transition between the high and low values of the mobility is expected to be fairly abrupt as the band-gap edges are approached, and is often called the mobility edge. There is little direct and unambiguous experimental evidence for the presence of this abrupt mobility edge, and the change in the transport properties near the band edges is not well known.

A related transport property that should exhibit a similarly abrupt transition is the efficiency-mobility-lifetime product ($\eta\mu\tau$). The product $\mu\tau$ represents the drift range per unit field of the excited carrier during its lifetime τ, and η represents the efficiency of excited carrier generation contributing to the current. For instance, η would account for surface recombination of photoexcited carriers and is not strongly dependent on energy. For states deep within the valence band and conduction band, $\eta\mu\tau$ is expected to be large, while in the band gap, $\eta\mu\tau$ is expected to be small. A major aspect of this study is to explore the energy dependence of $\eta\mu\tau$ for electrons and holes in hydrogenated amorphous silicon (*a*-Si:H).

One method for determining $\eta\mu\tau$ involves measuring the photoconductivity of *a*-Si:H as a function of exciting photon energy and intensity. Depending on the type of electrical contacts, two different modes of photoconductivity are observed: primary and secondary.[1,2] Primary photoconductivity occurs when the photoexcited carrier (either electron or hole) traverses the film no more than once because the electrodes cannot inject additional carriers to maintain charge neutrality. Secondary photoconductivity occurs when more photoexcited carriers (electrons and holes) can traverse the film than the number of photons absorbed because the electrodes can replenish the carrier by injection. Some electrode configurations may exhibit secondary photoconductivity for one carrier and primary photoconductivity for the other.

Three different experimental configurations are used to measure the photoconductivity. Each method depends on different aspects of transport and the optical absorption of *a*-Si:H. The most common photoconductivity measurement is made by photoexciting carriers between two electrodes on the surface or interface of the film. The gap electrode geometry yields the ambipolar secondary photoconductivity.[3-8] In this measurement, gap electrodes do not block either carrier. Hence, the photoconductivity is due to the secondary photocurrent of both carriers and will be denoted by SSPC (i.e., secondary electron and secondary hole photoconduc-

tivity). SSPC measures the sum of the $\eta\mu\tau$ for the electron and for the hole. A less commonly used photoconductivity measurement is unipolar secondary or secondary photoconductivity measured on a forward biased Schottky barrier.[2,8–10] In this measurement, the electrodes are on the top and bottom of the film. The secondary photocurrent of the electron dominates the primary photoconductivity of the holes because the Schottky barrier blocks holes. SPPC will be used to denote photoconductivity measured with this configuration and depends solely on the electron $\eta\mu\tau$. Finally, the photoconductivity measured on a reverse-biased Schottky barrier (denoted by PPPC) is due to the primary photocurrent of both carriers.[2,8–10] PPPC measures the $\eta\mu\tau$ of the hole.

The photoconductivity measurements do not give unique results for $\eta\mu\tau$ if the optical absorption is unknown because the different types of photoconductivity measure different transport properties and depend on the optical absorption. Some studies using primary and secondary photoconductivity have concluded, using traditional optical measurements, that $\eta\mu\tau$ varies with photon energy[2–4,9] while others show, or more often assume, that $\eta\mu\tau$ is constant with energy.[5–8,10] In addition, recent results have shown that the photoconductivity spectra changes as the band bending and surface conditions are altered,[11] resulting in erroneous determinations of the energy dependence of $\eta\mu\tau$.

The spectral region that is most important for analysis of the transport in *a*-Si:H extends from the optical band edge to deep within the gap. Conventional optical-absorption measurements, however, are least reliable in this region.[12] Since typical films (less than 5 μm thick) have absorptances of 10^{-4} at subband-gap energies and elastically scatter light, conventional reflection and transmission techniques are not adequate for determining the absorption spectra. Recently, the technique of photothermal deflection spectroscopy[13] (PDS) has been developed, which enables the reliable measurement of optical absorptions as small as 0.1 cm^{-1} for 1-μm-thick films. Furthermore, the PDS measurements are independent of the transport properties of the films and are insensitive to light scattered elastically from film inhomogeneities.[14] Previously, this technique had been employed to measure subband-gap and band-edge optical absorption for undoped, boron-doped, phosphorus-doped, and compensated *a*-Si:H films.[15]

Results are presented here which combine PDS absorption data with three types of photoconductivity measurements to derive $\eta\mu\tau$, for the electron and hole, as a function of photon energy in the range of 0.7–2.1 eV and to determine which states are involved in optical transitions.[16] It is shown that $\eta\mu\tau$ for electrons and holes exhibit different spectral dependences. The products $\eta\mu\tau$ for the electron and for the hole are both roughly independent of energy at short wavelengths, but at long wavelengths they commence a sharp decrease at different energies. A tentative model is proposed to explain the results. Finally, we demonstrate a method by which absorption spectra may be obtained from photoconductivity using constant generation rate normalization. However, we conclude that photoconductivity derived absorption spectra can have a fairly large uncertainty in the magnitude of the subband-gap shoulder due to defects and the slope of the exponential tail.

The outline of the paper is as follows. The sample geometry used for the different measurements and the experimental techniques are described in Sec. II. In Sec. III the physics and theory of the different types of photoconductivity are briefly discussed, and the prescription for constant generation rate normalization for photoconductivity is set forth. Section IV contains the experimental results, and Sec. V discusses the results in terms of a density-of-states model.

II. EXPERIMENTAL METHODS

Most of the *a*-Si:H films were prepared by rf glow discharge decomposition of pure SiH_4 onto quartz and 7059 glass substrates held at a deposition temperature of 230 °C.[17] These deposition conditions are known to produce low-defect films. Phosphorus-doped films were produced by mixing 10^{-3} parts PH_3 in SiH_4. All films were 2 μm thick.

The sample structures used for PDS and SSPC measurements were produced by first depositing 0.5-mm-long, 1000-Å-thick Ni electrodes on quartz substrates with a gap of 1.5 mm. Then a 2-μm layer of *a*-Si:H was deposited over the electrodes. The Schottky barrier structures used in this experiment were made by depositing 1000 Å of Ni on a glass substrate followed by a 300-Å n^+ layer to produce an ohmic contact. The 2-μm *a*-Si:H layer for both the Schottky barrier and the gap structure was deposited at the same time, ensuring that both structures contain identical *a*-Si:H. Finally, after less than 30 min of exposure to air, a 60-Å Pd or Pt semitransparent top electrode was deposited on the undoped and doped material.

Two dc discharge samples with gap electrodes (from RCA) were also used. The contacts were Cr with an n^+ layer. One sample was undoped and produced at a substrate temperature of 270 °C. The other was doped with 0.19 mol % PH_3 in the gas phase. The gap geometry results obtained on the dc discharge samples were the same as those obtained

on samples deposited by rf decomposition. Because the experimental setup used in the four measurements is similar, those features common to more than one measurement are described first, followed by those details unique to each specific measurement.

For the four types of measurements, the monochromatized ouput (13-nm resolution) of a 1000-kW Xe lamp illuminated the sample through a common optical system. The source intensity was measured by a pyroelectric detector. For ac measurements (PDS and SSPC with a dc bias light), the light was chopped by a mechanical chopper, and the signal was measured by a lock-in amplifier connected to a computer. For the dc measurements (all photoconductivity measurements except SSPC with a dc bias light), a computer-controlled mechanical shutter was placed in the beam. The current was measured by a current preamp, and the output of the preamp was averaged using an analog-to-digital converter interfaced to the computer. The dark current was averaged for periods up to 100 s with the light blocked, following a waiting period to ensure that equilibrium had been reached. The beam was then unblocked, and after a similar waiting period, the current was averaged while the film was illuminated. The photocurrent was computed by taking the difference between the two measurements. During the signal averaging, the incident light intensity was also averaged. For all the photoconductivity measurements, the intensity dependence of the photocurrent was measured at energies above and below the band gap and over as large an intensity variation as the signal-to-noise ratio would permit (up to 7 orders of magnitude). The intensity of the exciting light was varied by using calibrated neutral density filters. The subsequent analysis was performed on a Digital Equipment Corporation PDP computer.

In addition to the general experimental details mentioned above, there are a number of considerations specific to each of the four measurements. The PDS measurements were performed on the gap electrode samples by positioning the probe beam in the center of the gap. While some light was incident on the electrodes, the electrodes were roughly 100 thermal lengths away from the probe beam for an 8-Hz chopping frequency. This distance ensured that no signal came from light absorbed in the electrodes. An absorption spectrum measured on a sample without electrodes was identical to a spectrum obtained with electrodes, providing additional evidence that the PDS signal came from the film. The PDS measurements were made after the SSPC measurements, to ensure that the CCl_4 did not alter the bending of the bands. Over the spectral range measured, the PDS signal did not show any phase shifts indicating substrate, electrode, or liquid absorption.

The dc SSPC measurements were made with a 100-V bias where the I-V characteristics were quite linear. The electrode gap was uniformly illuminated with light either through the substrate or through the top surface. No significant difference in the (0.7—2.4)-eV range was observed. For SSPC measurements with a dc bias light, the output of a 150-W quartz-tungsten lamp illuminated the sample while the ac photocurrent was measured. The photocurrent from the dc bias light was over an order of magnitude greater than the ac photocurrent from the exciting light source at all photon energies. This reduced shift of the quasi-Fermi-level as the energy generation rate of the exciting light was varied.

The dc PPPC was measured at a -3-V reverse bias where the Schottky barrier exhibited saturation. The saturation of the photocurrent at -3-V reverse bias for undoped films and drift mobility experiments indicated that the depletion width extended through the sample.[9] The phosphorus-doped Schottky barriers did not show good rectifying I-V characteristics, and consequently, no photoconductivity results from these samples will be reported.

The dc SPPC was measured at 1.0-V bias. Because the response time was exceedingly long (greater than 3 s at low generation rates), care was taken to ensure that the photocurrent reached equilibrium before averaging commenced. Because of the sublinear dependence of the photocurrent on intensity, spectra were taken at different intensities to verify the normalization procedure (see Sec. III E).

III. THEORY

This section contains formulas describing PDS, SSPC, SPPC, and PPPC and a brief description of the physical processes involved in each measurement. The problems of correctly normalizing the photoconductivity to derive $\eta\mu\tau$ are also discussed.

A. Photothermal deflection spectroscopy

The physical principle behind PDS is straightforward. When an intensity-modulated light beam is absorbed by a sample, periodic heating of the sample and the surrounding media occurs. A HeNe probe laser grazing the sample will experience a periodic deflection due to the index-of-refraction gradient caused by the sample heating. The beam deflection synchronous with the intensity-modulated beam is detected by a position sensor connected to a lock-in amplifier. The beam deflection is measured as a function of the wavelength of the intensity-modulated beam.

The optical properties of the absorbing material are related to the normalized photothermal deflec-

tion signal S by[13]

$$S=D/D_0=(1-R)(1-e^{-\alpha t}) \quad (1)$$

for thermally thin films where D is the deflection per incident power, D_0 is the maximum deflection per incident power determined from the saturation of the PDS signal at high energies where the beam is completely absorbed, R is the surface reflectivity of the film, α is the absorption coefficient, and t is the sample thickness. Equation (1) has the physical interpretation that the beam deflection is directly proportional to the absorbed power.

B. Secondary gap photoconductivity

The photoconductivity depends on both the absorbed power and the transport. First consider secondary photoconductivity in the gap configuration. Because a large bias is applied across the electrodes and the large resistance of the a-Si:H film, most of the field drops uniformly across the film rather than the contacts [see Fig. 1(a)]. Furthermore, both electrons and holes can be injected into the material from the contacts to maintain charge neutrality of the film. Hence it is possible to have more electrons and holes transitting the film than absorbed photons, i.e., photoconductive gain.

In the case of SSPC, the photocurrent $(\Delta I)_{SS}$, is given by

$$(\Delta I)_{SS}=[(\eta\mu\tau)_e+(\eta\mu\tau)_h]efVtw/L \ , \quad (2)$$

where

$$f=F(1-R)(1-e^{-\alpha t})/t \quad (3)$$

is the average number of photons absorbed per cubic centimeter per second, F is the flux of photons per $cm^{-2}s^{-1}$, t is the film thickness, w is the electrode width, η is the quantum efficiency of carrier generation, τ is the free-carrier lifetime, μ is the free-carrier mobility, V is the applied voltage, L is the distance between electrodes, and e is the electron charge. The subscripts e and h refer to electrons and holes, respectively. From Eq. (1), one obtains

$$f=FS/t \ . \quad (4)$$

C. Secondary forward-bias photoconductivity

For Schottky barriers in forward bias, the secondary photocurrent is only due to electrons rather than both electrons and holes as in the gap cell geometry. Figure 1(b) illustrates that when an electron reaches the electrode, a new electron can be injected through the ohmic back contact to maintain charge neutrality of the film. The hole, however, cannot be replenished when it reaches the ohmic contact since the Schottky barrier prevents hole injection. For Pd on undoped a-Si:H, the Schottky barrier height for electrons is 0.96 eV.[18] Assuming a 1.75-eV band gap, the Schottky barrier results in a $\sim$0.8-eV barrier to the injection of holes. Hence the photocurrent is dominated by the transport of the electron.

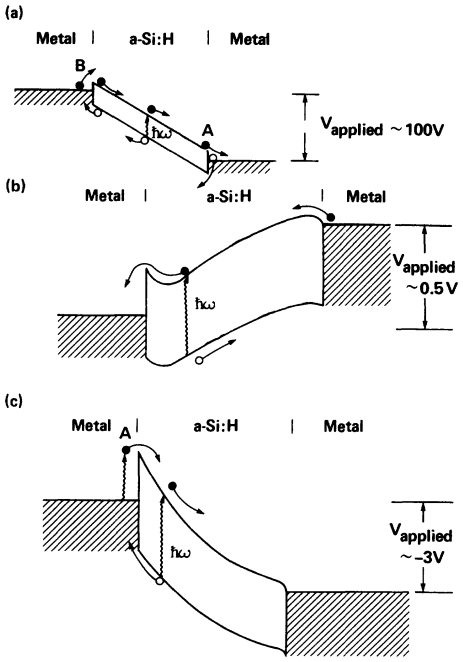

FIG. 1. (a) Secondary gap photoconductivity (SSPC). Both electrons and holes can be injected into the material by the contacts. If an electron (hole) leaves the film at A (B), a new one is injected at B (A) to maintain charge neutrality of the film. Transport depends on both electron and holes. (b) Secondary forward-bias photoconductivity (SPPC). The ohmic back contact can inject electrons but the Schottky barrier cannot inject holes. Transport depends only on the electron. (c) Primary reverse-bias photoconductivity (PPPC). Neither electrons nor holes can be injected in this configuration. Consequently, an electron is collected only if a hole is also transported to the contact. Transport is limited by the carrier with the minimum transport (the hole). The transition A gives rise to internal photoemission.

The secondary forward-bias current is given by

$$(\Delta I)_{SP}=ef(\eta\mu\tau)_e VA/t \ , \quad (5)$$

where A is the contact area. It should be noted that f must be corrected for the reflectivity and absorption of the front and back contact. This correction is only very weakly dependent on energy.

D. Primary reverse-bias photoconductivity

The photocurrent of the reverse-biased Schottky barrier measures the number of collectible electron-hole pairs. As illustrated in Fig. 1(c), the electrons generated in the depletion width are transported to the ohmic back contact while the hole travels to the Schottky barrier. Because the ohmic contact cannot inject holes, while the Schottky barrier cannot inject electrons, the photocurrent is equal to the number of electron-hole pairs generated within the depletion width. No additional carriers can be injected through the contacts. Consequently, the photocurrent is limited by the carrier with the smallest $\mu\tau$ or range.

For a-Si:H, the hole has the smallest $\mu\tau$ in the (0.7—2.5)-eV energy region. This is demonstrated by comparing SSPC with SPPC (discussed later) and drift mobility experiments, which show that $(\mu\tau)_e$ is at least 5 times larger than $(\mu\tau)_h$.[19] The reverse-bias photocurrent, $(\Delta I)_{\rm PP}$, is limited by the number of holes collected. Thus, ignoring contributions due to electrons, we find

$$(\Delta I)_{\rm PP}=e(1-e^{-\alpha X})(1-R)FA\eta_h$$
$$=e\{1-[1-S/(1-R)]^{X/t}\}FA(1-R)\eta_h\ , \tag{6}$$

where X is equal to the minimum of $\{t,(\mu\tau)_h V/t\}$ is the hole depletion width and depends on the photon energy. For small absorptances ($S\ll 1$) or when the sample is fully depleted ($X\simeq t$),

$$(\Delta I)_{\rm PP}\simeq(\eta\mu\tau)_h eFSVA/t^2 \tag{7}$$

or

$$(\eta\mu\tau)_h\simeq(\Delta I)_{\rm PP}t^2/(eFSVA)\ . \tag{8}$$

Equation (8) is valid for the entire energy range for undoped samples since below 1.8 eV, $S\ll 1$, and above 1.8 eV, $X\simeq t$. For photon energies greater than 1.8, two observations show that $X\simeq t$. The reverse-bias photocurrent saturates as a function of increased reverse bias,[2] and the PPPC spectra saturate at the same α as the PDS measurements.

There is, however, the additional contribution of internal photoemission in the reverse-bias Schottky barrier illustrated by transition A in Fig. 1(c).[20] The expected form for the photoemission current $(\Delta I)_{\rm pe}$ for $\hbar\omega$ less than the band gap is given by

$$(\Delta I)_{\rm pe}/\hbar\omega=C(\hbar\omega-V_B)^2\ , \tag{9}$$

where C is some constant, and V_B is the barrier height. This contribution appears below the band-gap energy of the semiconductor and depends on the contact metal.

E. Photoconductivity normalization

Steady-state photocurrent depends on the occupation of traps and recombination centers as well as the carrier-transport properties. Therefore, the change of occupation due to varying generation rates must be taken into account as the energy of the exciting light is varied. The ideal photoconductivity experiment would be to measure the dc current caused by a very weak exciting beam. Such an experiment would not significantly alter the occupation of the gap states from equilibrium and would not be affected by long photoconductive response times. The advantage of using the dc measurement is that the current carriers are in equilibrium with all the states in the gap. Unfortunately, such a measurement is difficult to perform because the dark current can be much larger than the photocurrent.

To overcome this problem, a normalization procedure has been developed which encompasses a constant generation normalization and relies on the absorption coefficient measured by PDS, the intensity dependence of the photocurrent, and the spectral dependence of the photocurrent. To accomplish the normalization, dc measurements of the photocurrent were performed to eliminate response-time effects, and the intensity dependence was measured over a wide range of incident fluxes for several fixed photon energies spanning the wavelength region. For a fixed photon energy, we define a function $g(f)$ by

$$g(f)=\Delta I/(f)/\Delta I/(f_0)\ , \tag{10}$$

where $\Delta I/(f)$ is the photocurrent at generation rate f and f_0 is an arbitrary but fixed generation rate. $g(f)$ is determined by dividing the photocurrent versus flux curves by the reference photocurrent and using Eq. (4) to calculate f. Except for a constant factor, $g(f)$ does not depend significantly on energy. [If $g(f)$ is approximately given by $g(f)\simeq f^\gamma$, γ varies by less than the experimental error of 0.07.] Hence Eq. (10) can be used to compute the photocurrent at one generation rate given the photocurrent at a different rate for all wavelengths. In order to further minimize possible errors due to any small dependence of $g(f)$ on photon energy, the intensity of the exciting light was adjusted so that the photocurrent was less than the dark current. The generation rate did not vary by more than 1 order of magnitude.

The resulting normalized photoconductivity spectra are independent of intensity changes of over 3 orders of magnitude. Figure 2(a) shows SSPC per incident flux with a 1-V forward bias for several different intensities. After constant generation rate normalization, the photocurrent is independent of intensity, as shown by the solid line in Fig. 2(b) which contains all the data points in Fig. 2(a). This

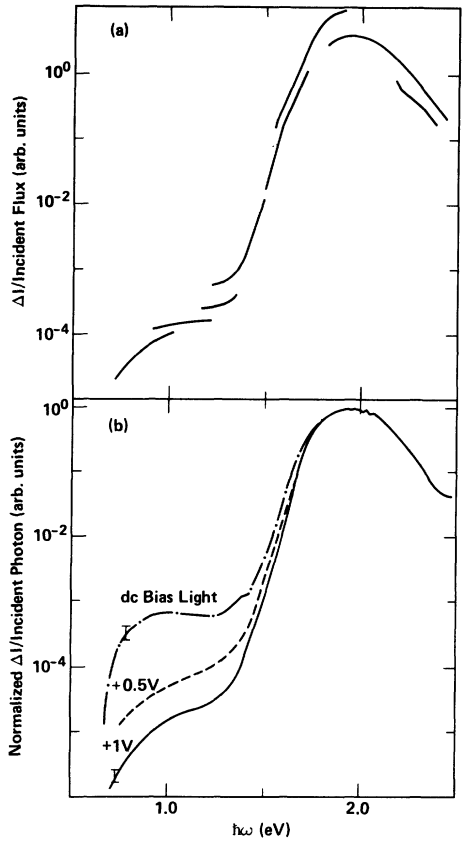

FIG. 2. (a) Secondary forward-bias photocurrent (SPPC) per incident flux for 1-V forward bias. Breaks are due to various attenuations of the exciting light. (b) —, constant generation rate normalization of the 1-V forward-bias photocurrent in (a). Note that the different intensities are now superimposed. ---, constant generation rate normalization of 0.5-V forward-bias photocurrent. -·-, ac SSPC with a dc bias light.

is conclusive demonstration that the constant generation rate normalization procedure removes the intensity dependence from the spectra.

These spectra are used to calculate $\eta\mu\tau$ for a constant generation rate using Eqs. (2)—(5) and (10). We obtain for SSPC

$$(\eta\mu\tau)_e+(\eta\mu\tau)_h=(\Delta I)_{\rm SS}L/[g(FS/t)ef^0Vtw]\ , \tag{11}$$

and for SPPC

$$(\eta\mu\tau)_e=(\Delta I)_{\rm SP}t/[g(FS/t)ef^0VA]\ . \tag{12}$$

Equation (8) can be used to derive $(\eta\mu\tau)_h$ without the constant generation rate correction because the reverse-bias primary photoconductivity shows a linear intensity dependence.

An alternate approach to the constant generation rate normalization is to illuminate the sample with above-gap dc bias light of intensity much greater than the ac probe light.[10] The dc bias light introduces so many carriers that the occupation of the gap states is not significantly altered by the ac probe beam. The need for a dc measurement is reduced since equilibrium with gap states should occur rapidly due to the large number of carriers. This technique was not used extensively in this experiment because of the following difficulties. First, there is an interaction between the dc bias light beam and the ac exciting beam. The ac exciting beam not only modulates the number of carriers, but also modulates the trap and recombination center occupation. Modulation of these levels can significantly modulate the much larger photocurrent from the dc bias light, giving rise to either quenching or enhancement of the photocurrent.[21] In some samples, this modulation can be significant. Second, the occupation of the gap states may be significantly altered from thermal equilibrium. The altered occupation gives rise to photoinduced absorption, and the $\eta\mu\tau$ measured under such circumstances is not an equilibrium value but rather the $\eta\mu\tau$ for a highly excited material. Third, measurements demonstrated that even when the bias light was an order of magnitude greater than the ac light, the ac photocurrent had small but significant phase shifts at low energies, indicating that lifetime effects were still important. The ac photocurrent had an intensity dependence of $F^{0.9}$. This sublinearity, if uncorrected, results in significant errors in the exponential edge and in the defect photoconductivity relative to the above band-gap photoconductivity [see Fig. 2(b)]. Finally, the large generation rate of the dc bias light shrinks the depletion width and is unsuitable for examining the effects of band bending.[11] While these problems can be minimized, they are sufficiently worrisome to warrant the alternative of constant generation rate normalization.

IV. RESULTS

The results of PDS, SSPC, SPPC, and PPPC divided by the incident flux for the undoped films are shown in Fig. 3. Note that the exponential edges and defect peaks differ markedly. In Fig. 4, we show the corresponding intensity dependence of the photocurrent at the wavelength of 660 nm. The curves in Fig. 4 are then used to normalize the photoconductivity spectra shown in Fig. 3 to a constant generation rate according to the prescription in Sec. III E. The results are shown in Fig. 5. The agreement among the absorption, secondary gap, and sandwich photoconductivity is much better after

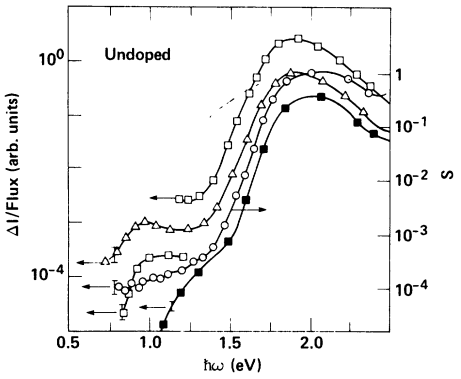

FIG. 3. Photoconductivity and absorptance of undoped *a* -Si:H. -○-, PDS measurement of absorptance. -△-, secondary gap photoconductivity (SSPC). -□-, secondary forward bias photoconductivity (SPPC). The break shows the effect of attenuating the exciting beam by 1000 for photon energies above 1.25 eV. -■-, primary reverse bias photoconductivity (PPPC). Decrease at high energies is due to the increasing reflectivity of the sample, surface recombination, and/or back diffusion of the carriers.

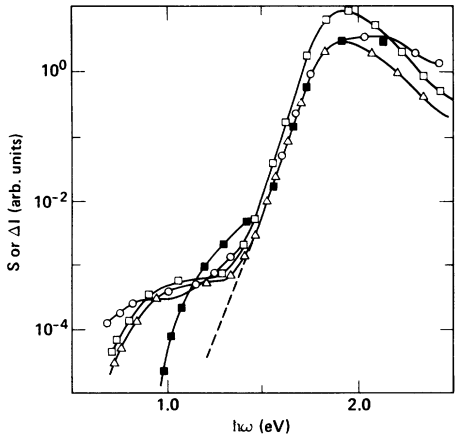

FIG. 5. Constant generation rate normalized photoconductivity and absorptance vs photon energy (derived from data in Figs. 3 and 4 and the equations in Sec. III E). Symbols are the same as in Fig. 3. Note that the discontinuity in SPPC due to the change in intensity has disappeared. The dotted line shows the primary reverse-bias photoconductivity without the internal photoemission contribution.

constant generation rate normalization. The above-gap edges and magnitude of the defect shoulder match well.

The structure below 1.5 eV in the PPPC curve is due to internal photoemissions. With the use of Eq. (9), the square root of the yield plotted versus photon energy should give a straight line with the barrier height given by the intercept. This is plotted in Fig. 6, and the intercept indicates a barrier height of 0.96 eV. This value is in excellent agreement with the value 0.95 eV found by analyzing the temperature dependence of the *I-V* characteristics.[18] Also, if the transparent contact is changed to Pt, the shape of the structure changes. Consequently, Eq. (9) can be used to subtract the internal photoemission contribution. The result is shown by the dotted line in Fig. 5 and is used in the computation of $(\eta\mu\tau)_h$.

Using Eqs. (8), (11), and (12), one can derive $(\eta\mu\tau)_h$, $(\eta\mu\tau)_e+(\eta\mu\tau)_h$, and $(\eta\mu\tau)_e$, respectively. In Fig. 7, $(\eta\mu\tau)_e$ and $(\eta\mu\tau)_e+(\eta\mu\tau)_h$ are plotted as a function of photon energy for an undoped film. The error bars in the (1.0—1.5)-eV region are due to the uncertainties in the photoconductivity normalization. Below 0.9 eV, the errors are dominated by the PDS results for undoped samples. There is an absorption band due to OH in the substrate at ~0.8—0.9 eV which must be subtracted for the

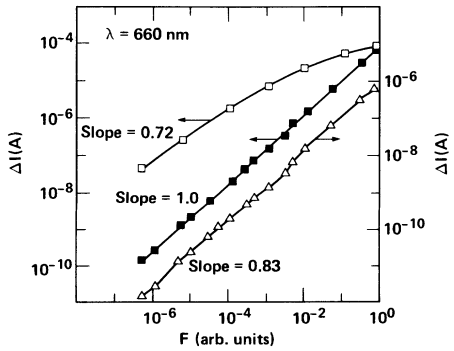

FIG. 4. dc photocurrent vs light flux F at a wavelength of 660 nm. -□-, SPPC; -△-, SSPC; -■-, PPPC.

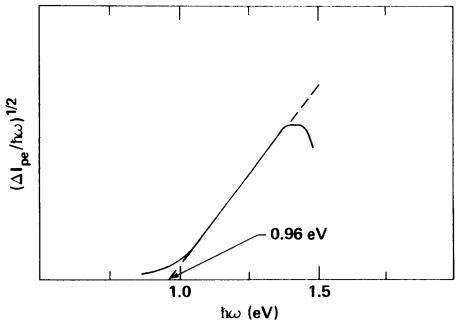

FIG. 6. Plot of the square root of the photocurrent per incident photon vs photon energy. Extrapolated barrier height V_B is 0.96 eV.

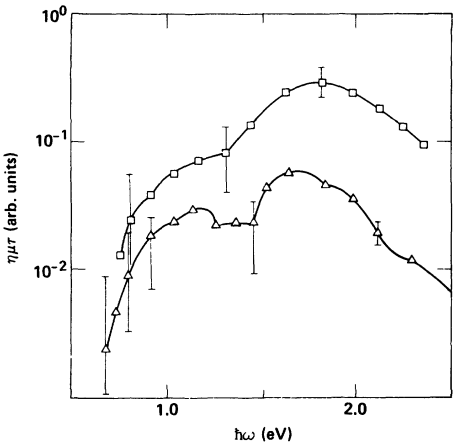

FIG. 7. $\eta\mu\tau$ derived from photoconductivity and absorptance. -△-, $(\eta\mu\tau)_e+(\eta\mu\tau)_h$ from SSPC. -□-, $(\eta\mu\tau)_e$ from SPPC. The curves are offset from one another for clarity. The error bars indicate the uncertainty of the low energy points (less than 1.5 eV) relative to 2.0 eV. Dropoff at high energies is due to surface recombination and back diffusion.

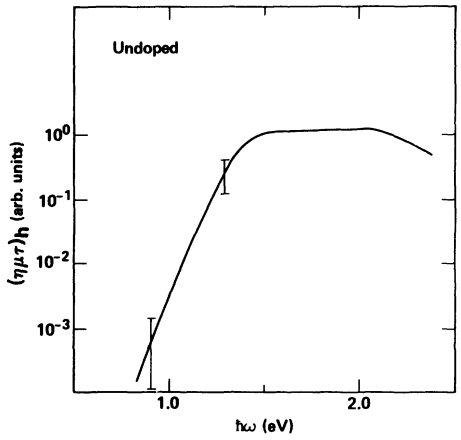

FIG. 8. $(\eta\mu\tau)_h$ relative to the value at 2.0 eV vs photon energy. Error bars are due to the presence of internal photoemission. Dropoff at high energies is due to surface recombination and back diffusion.

low-defect undoped samples. Within the error bars of the experiment, the holes do not contribute significantly to the photocurrent throughout the energy range. This result follows from the data showing that $(\eta\mu\tau)_e$ and $(\eta\mu\tau)_e+(\eta\mu\tau)_h$ have the same energy dependence (see Fig. 7), and the fact that the photocurrent is predominantly carried by electrons for above-band-gap illumination at room temperature. We see that $(\eta\mu\tau)_e$ is essentially constant until 0.9 eV, after which a fairly rapid decrease occurs. The decrease $(\eta\mu\tau)_e$ at high photon energies is due to back diffusion in the case of SPPC and surface recombination for SSPC. Because these results demonstrate that the hole has the smaller range, the assumptions made to derive Eq. (8) are justified.

The $(\eta\mu\tau)_h$ versus energy is shown in Fig. 8, and the contribution to internal photoemission has been subtracted. There is a very large decrease in $(\eta\mu\tau)_h$ below 1.5 eV, indicating that the hole is becoming very localized. The presence of internal photoemission makes any residual primary photocurrent difficult to detect and gives rise to the large error bars.

Figure 9 shows the absorptance from PDS and SSPC per unit flux for the phosphorus samples. Using constant generation rate normalization for the photoconductivity and the PDS results, one obtains $(\eta\mu\tau)_e$ versus energy for phosphorus doping. The hole lifetime and mobility are very small in phosphorus-doped material, resulting in a negligible hole contribution to the photocurrent. Because the absorption in phosphorus-doped samples is so much larger than in undoped a-Si:H, the substrate OH absorption peak is not a problem. Hence the error bars below 0.9 eV are smaller, and the drop in $(\eta\mu\tau)_e$ is significant below 0.9 eV.

V. DISCUSSION

The model described below is derived from the above data. In the following discussion, it is convenient to divide the spectra into three regions: region A, $\hbar\omega > 1.5$ eV; region B, $0.9 < \hbar\omega < 1.5$ eV; region C, $\hbar\omega < 0.9$ eV.

Figure 10 depicts the approximate density of states for undoped and phosphorus-doped material, as measured by deep-level transient spectroscopy,[22]

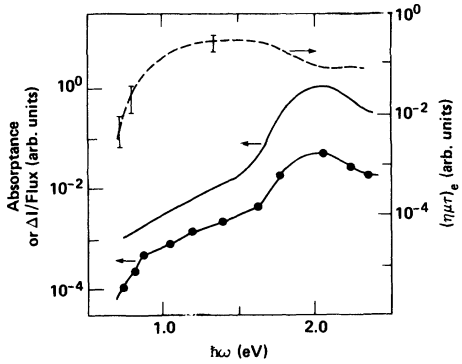

FIG. 9. Results for 10^{-3} phosphorus-doped sample. —, absorptance measured by PDS. -●-, secondary gap photocurrent per incident flux. ---, $(\eta\mu\tau)_e$ using constant generation rate normalization. Error bars represent errors relative to the 2.0-eV value.

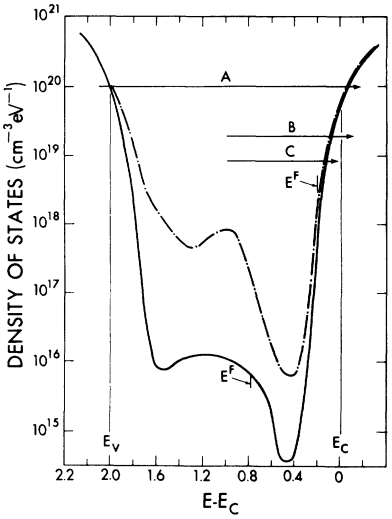

FIG. 10. Density of states for undoped and P-doped films are measured by capacitance deep-level transient spectroscopy (Ref. 22) and dispersive transport (Ref. 23). States are localized for energies between E_v and E_c. The labeled transitions give rise to photoconductivity for the different energy regions described in the text.

dispersive transport,[23] and optical-absorption measurements.[24] Recent absorption measurements have shown that the density-of-states maximum above the valence band (Fig. 10) is due to dangling silicon bonds for undoped and phosphorus-doped material.[15,24]

In region *A*, the transitions in both phosphorus-doped and undoped films are band-to-band transitions resulting in free or shallow trapped electrons and holes. These trapped carriers can be thermally excited above the mobility edges. In SSPC, the current is carried by the electrons because of their greater $(\eta\mu\tau)_e$. In PPPC, the mobility of the holes is sufficient to allow collection of most of the holes within a depletion width, which in our case extends throughout the film. Consequently, the absorption, SSPC, and PPPC show the same wavelength dependence.

In region *B*, the transitions are primarily from the gap state maximum to the conduction band. The generated electrons conduct above the conduction-band mobility edge. Because most of the current is carried by electrons in regions *A* and *B*, the absorption, SSPC, and SPPC exhibit a similar energy dependence. The $(\eta\mu\tau)_h$ becomes small because the hole becomes localized for energies less than 1.5 eV. This limits the primary reverse-bias photoconductivity. Consequently, in region *B* the PPPC becomes small relative to the absorption and secondary photoconductivity.

Finally, in region *C*, light does not generate either mobile holes or electrons for undoped and phosphorus-doped films, causing all three types of photoconductivity to decrease relative to the absorption. The optical absorption remains high due to transitions between localized states. Since the localized states in the tail immediately below the mobility edge can have a spatial extent larger than 1 nm, there can be a non-negligible transition probability. This is supported by the fact that localized state absorption has been found in the case of amorphous arsenic.[25]

The localization of holes produced by light of energy less than 1.5 eV is consistent with other results. The mobility gap (the energy between the mobility edges of the conduction and valence bands) is estimated to be $\sim 1.7-1.9$ eV. In this material, the hole lifetime is estimated to be 10^{-7} s.[12,26] At room temperature, assuming an attempt frequency of 10^{13} s^{-1}, holes as deep as 0.3 eV above the valence-band mobility edge can be thermally excited to the mobility edge. Consequently, light less than $\sim 1.4-1.6$ eV will not generate a primary photocurrent. Recent results on photocells suggest a photovoltaic gap of 1.5 eV.[27] The photovoltaic gap energy is consistent with the results found in this experiment which show that the gap energy is due to the localization of holes.

The results in Figs. 7 and 9 are somewhat different than previous measurements of the energy dependence of $(\eta\mu\tau)_e$.[3,4,7] The earlier results show a large decrease in $(\eta\mu\tau)_e$ below ~ 1.5 eV. There are two reasons for this discrepancy with previous measurements. First, the optical absorption was measured by transmission and reflection, which will overestimate the absorption because of scattering and result in a drop in $\eta\mu\tau$. In addition, realistic error bars associated with previous measurements of $\eta\mu\tau$ are roughly as big as the decrease below 1.5. Second, previous photoconductivity measurements were not corrected for constant generation rate normalization, distorting the energy dependence of $(\eta\mu\tau)_e$. The more accurate results of this experiment show that $(\eta\mu\tau)_e$ is constant to 0.9 eV.

The fact that $(\eta\mu\tau)_e$ is constant implies that the absorption shoulder below 1.5 eV is due to transitions from states within the gap to the conduction band rather than from the valence band to gap states. Since the band-to-band transitions and the defect transitions have the same $(\eta\mu\tau)_e$, the final state (the conduction band) must be the same. The energy threshold of the absorption shoulder is a measure of the energy from the defect level to the conduction band, confirming the recent interpretation of the absorption spectra.

The energy independence of $(\eta\mu\tau)_e$ suggests that,

in principle, photoconductivity can be used to measure the absorption down to 0.9 eV. In practice, photoconductivity measurements are subject to considerable variations and require great care to derive a quantitative absorption spectra. The gap photoconductivity results vary enormously depending on the previous thermal and optical history of the sample, as well as conditions of band bending. The forward-bias secondary-photoconductivity spectra depend on the previous history of the sample and on properties of the contacts. If one operates at a very large forward bias, the above-band-gap photoconductivity becomes enhanced relative to the subband-gap photoconductivity. This is demonstrated in Fig. 2(b) where the 1-V forward-bias spectra is a factor of 2 lower than the 0.5-V spectra. These effects most likely occur because of the injection properties of the contacts and space charge at high currents. Comparisons of the highly reproducible PDS results to the variable results of photoconductivity indicate that the subband-gap photoconductivity is only accurate to within a factor of 2 to 3 relative to the above-gap photoconductivity. This implies that the slope of the absorption edge deduced from photoconductivity may be off as much as 15% or roughly 10 meV in samples with low defect densities.

The results resolve the question of whether primary or secondary photoconductivity is a better measure of the absorption. The primary photocurrent below the absorption edge is dominated by the internal photoemission and the short range of the hole. Hence primary photoconductivity is not an accurate measure of the defect absorption tail. The lifetime effects in primary photoconductivity, however, are much less of a problem than in secondary photoconductivity. Primary photoconductivity is, therefore, better for measuring the slope of the absorption edge. Measuring the absorption using photothermal defection spectroscopy is faster, requires less specialized sample preparation, and is more reliable than measuring the absorption using photoconductivity.

VI. CONCLUSIONS

Results have been presented comparing the optical absorption, measured by photothermal deflection spectroscopy to secondary gap photoconductivity, sandwich photoconductivity, and primary photoconductivity for undoped and phosphorus-doped hydrogenated amorphous silicon films. We demonstrated a constant generation rate method for normalizing photoconductivity when the photocurrent depends nonlinearly on the intensity. The electron efficiency-mobility-lifetime product was found to be roughly independent of photon energy in the range $\sim 0.9-2.2$ eV for both undoped and phosphorus-doped samples. For energies less than ~ 0.9 eV, the electron efficiency-mobility-lifetime product dropped rapidly, especially for phosphorus-doped samples. The hole efficiency-mobility-lifetime product abruptly decreased for holes produced by photons of energy less than 1.5 eV. The energy independence of the $(\eta\mu\tau)_e$ leads to the conclusion that the subband-gap absorption shoulder is due to transitions from a defect level within the gap to the conduction band. The experiments demonstrated that secondary photoconductivity is a better qualitative measure of the gap state absorption than primary photoconductivity. Finally, the problems and accuracy of photoconductivity derived spectra were mentioned.

ACKNOWLEDGMENTS

We would like to thank R. Crandall for suggesting the shutter method for measuring the dc photoconductivity, R. Street, G. Moddel, N. Johnson, and M. Thompson for helpful discussions, and D. E. Carlson for providing some initial samples. This work was supported in part by the Solar Energy Research Institute under Contract Nos. XJ-O-9079-1 and DS-O-8107-1.

[1]For a review of photoconductivity, see R. H. Bube, *Photoconductivity of Solids* (Wiley, New York, 1964).
[2]R. S. Crandall, Sol. Cells 2, 319 (1980).
[3]P. J. Zanzucchi, C. R. Wronski, and D. E. Carlson, J. Appl. Phys. 48, 5227 (1977).
[4]T. D. Moustakas, Solid State Commun. 35, 745 (1980).
[5]G. Moddel, D. A. Anderson, and W. Paul, Phys. Rev. B 22, 1918 (1980).
[6]C. C. Tsai and H. Fritzsche, Sol. Energy Mater. 1, 29 (1979).
[7]R. J. Loveland, W. E. Spear, and A. Al-Sharbaty, J. Non-Cryst. Solids 11, 55 (1973).
[8]B. Abeles, C. R. Wronski, T. Tiedje, and G. D. Cody, Solid State Commun. 36, 537 (1980).
[9]R. S. Crandall, Phys. Rev. Lett. 44, 749 (1980).
[10]H. M. Welsch, W. Fuhs, K. H. Greeb, and H. Mell, J. Phys. (Paris) Colloq. 42, C4-567 (1981).
[11]D. G. Ast and M. H. Brodsky, Philos. Mag. B 41, 273 (1980); H. Fritzsche, Sol. Cells 2, 289 (1980); W. B. Jackson and M. J. Thompson, in Proceedings of the 16th International Conference on the Physics of Semiconductors (in press).

[12]For example, see references in H. Fritzsche, Sol. Energy Mater. 3, 447 (1980).
[13]W. B. Jackson, N. M. Amer, A. C. Boccara, and D. Fournier, Appl. Opt. 20, 1333 (1981); A. C. Boccara, D. Fournier, W. B. Jackson, and N. M. Amer, Opt. Lett. 5, 377 (1980); A. C. Boccara, D. Fournier, and J. Badoz, Appl. Phys. Lett. 36, 130 (1980).
[14]Z. Yasa, W. B. Jackson, and N. M. Amer, Appl. Opt. 21, 21 (1982).
[15]W. B. Jackson and N. M. Amer, Phys. Rev. B 25, 5559 (1982); W. B. Jackson and N. M. Amer, in *Tetrahedrally Bonded Amorphous Semiconductors (Carefree, Arizona),* A Topical Conference on Tetrahedrally Bonded Amorphous Semiconductors, edited by R. A. Street, D. K. Biegelsen, and J. C. Knights (AIP, New York, 1981), p. 263.
[16]Preliminary results were reported in W. B. Jackson and N. M. Amer, Lawrence Berkeley Laboratory Report No. LBL-13477 (unpublished).
[17]R. A. Street, D. K. Biegelsen, and J. C. Knights, Phys. Rev. B 24, 969 (1981).
[18]M. J. Thompson, N. M. Johnson, R. J. Nemanich, and C. C. Tsai, Appl. Phys. Lett. 39, 274 (1981).
[19]R. A. Street, Appl. Phys. Lett. 41, 1060 (1982).
[20]C. R. Wronski, B. Abeles, G. D. Cody, and T. Tiedje, Appl. Phys. Lett. 37, 96 (1980).
[21]P. D. Persans, Solid State Commun. 36, 851 (1980).
[22]D. V. Lang, J. D. Cohen, and J. P. Harbison, Phys. Rev. B 25, 5285 (1982).
[23]T. Tiedje and A. Rose, Solid State Commun. 37, 49 (1981).
[24]W. B. Jackson, Solid State Commun. 44, 477 (1982).
[25]J. C. Knights and J. E. Mahan, Solid State Commun. 21, 983 (1977).
[26]T. D. Moustakas, C. R. Wronski, and T. Tiedje, Appl. Phys. Lett. 39, 721 (1981).
[27]E. Yablonovitch and T. Tiedje, Bull. Am. Phys. Soc. 27, 268 (1982).